Soft Matter

View Online
Dynamic Article Links

Cite this: DOI: 10.1039/c1sm05142c

www.rsc.org/softmatter

PAPER

Self-assembly of semiflexible block copolymers: 2D numerical implementation of self-consistent field theory

Jie Gao, Wendi Song, Ping Tang* and Yuliang Yang

Received 27th January 2011, Accepted 8th March 2011
DOI: 10.1039/c1sm05142c

The phase behavior of rod-coil diblock copolymers is investigated in a two-dimensional positional space by using self-consistent field theory (SCFT) based on wormlike chain model. The segment orientation is defined on a unit spherical surface in three-dimensional space with an icosahedron triangular mesh and a finite volume algorithm is borrowed to numerically solve the Laplacian on the sphere. By taking advantage of 2D space calculation, the phase diagram including isotropic, nematic, smectic-A, smectic-C and further appended non-lamellar structures is constructed for the rod-coil diblock copolymers within the framework of Onsager excluded-volume interactions, in which microphase separation and liquid crystalline behavior are driven only by the entropy. Similar to our previous 1D space calculations, although smectic structures occupy large region in the phase diagram, tetragonal packed arrays of ellipse like domains in our 2D space simulations is observed at relatively high coil fractions and strong orientational interactions. We also reexamine the stability of zigzag and confirm it as a thermodynamically metastable structure of rod-coil copolymers in terms of the SCFT free energy.

Introduction

Rod-coil block copolymers have the ability of achieving well-defined long-range composition ordering nanoscale structures and specific orientational ordering due to the coupling of microphase and orientation interactions. Therefore, the self-assembly of rod-coil block copolymers has attracted much attention in recent years for enormous applications in a wide variety of technologies such as organic optoelectronics,[1–3] nanolithography,[4] biotechnology,[5–7] and high-performance resins,[8] in which chain rigidity originates from π-conjugation, helical secondary structure, or aromatic groups into polymer blocks.[9] For instance, optimization of organic photovoltaic and light emitting devices relies crucially on balanced charge injection and transport through the device, requiring the nanoscale morphology of at least two materials with different electron affinities to maximize charge separation, recombination and transfer. In this regard, nanostructures satisfying the requirement can be self-assembled by rod-coil diblock copolymers with rods and coils going respectively for acceptor and donor domains, which are thus economic and efficient way to fabricate highly efficient polymeric organic optoelectronics compared with conventional devices.[3] In the past couple of decades, a number of intriguing phases had been observed in rod-coil block copolymer solution or melt. Chen *et al.* observed morphologies characterized as "wavy", "arrowhead" and "zigzag" from polyhexyl isocyanate-polystyrene (PHIC-PS) rod-coil block copolymers by solvent-casting technique.[10,11] Radzilowski *et al.* observed unique structure transitions from lamellae to cylindrical phases and to hexagonally packed micellar phases in monodisperse rod-coil block copolymers with high coil volume fraction.[12,13] Besides that, a number of intriguing phases including straight lamellae,[14] perforated lamellae,[15–17] hexagonal stripes,[12–14] pucks,[16,18] spheres,[19,20] cylindrical,[21–23] and bicontinuous cubic[24–26] were detected in rod-coil block copolymers by using different techniques and experimental facilities.

Theoretical understanding of the phase behavior and self-assembly mechanism of rod-coil block copolymers is thus desirable. Self-consistent field theory (SCFT) has proven to be extremely valuable in understanding the phase behavior of traditional coil-coil block copolymers in intermediate segregation regions. The extension of SCFT to rod-coil systems, however, is quite limited. Most of these previous studies are based on either further assumptions of complete rigidity or ignorance of orientational interactions between rods.[27–29] In fact, the wormlike chain model is the most generic model to describe chain rigidity with the consideration of chain bending conformation.[30–36] In this model, the statistical distribution of a specific segment is determined by a chain propagator $q(\mathbf{r}, \mathbf{u}, t)$, which gives the probability of the t-th monomer to appear in the position $\mathbf{r}$ and point to direction $\mathbf{u}$. In contrast to Gaussian chains, the additive $\mathbf{u}$-dependence makes the diffusion equation of $q(\mathbf{r}, \mathbf{u}, t)$ more complicated, which has been a challenge in numerical SCFT study on semiflexible polymers. Duchs and

Key Laboratory of Molecular Engineering of Polymer, Ministry of Education, and Department of Macromolecular Science, Fudan University, Shanghai, 200433, China. E-mail: pingtang@fudan.edu.cn

Sullivan[31] proposed a spherical harmonic method to deal with orientation dependent physical quantities to explore the liquid crystal behavior of rod-coil system under the Onsager-type excluded-volume interactions. They performed SCFT calculations which assumed $m = 0$ in spherical harmonics expansion, *i.e.*, restricted their results to phases with axial-symmetries and constructed a phase diagram including smectic-A, nematic, and isotropic phases. Later in the paper by Hidalgo *et al.*,[32] the "end" effects omitted in their previous paper applicable to infinitely thin rods[31] were included. With the additional "end" effects taken into consideration, smectic-A phase was found at arbitrarily large rod volume fraction, while smectic phases does not occur when the rod-coil block copolymers become "homogeneous" rigid polymers in the limit of $f_R \rightarrow 1$ if the "end" effects are omitted.[37] Very recently, Jiang and Chen[34] investigated the interfacial properties between isotropic and nematic phases by using SCFT based on the worm-like chain model along with Onsager orientational interaction. This work improved a large step to numerically solve the modified diffusion equations by employing more accurate Crank-Nicholson algorithm. In this technique, the Laplacian on a unit sphere was obtained by taking advantage of a software package SPHEREPACK involving convenient analysis and synthesis of spherical-harmonics functions and inverted Laplacian. In our previous work,[35] we developed a novel real-space numerical implementation to solving the diffusion equation of $q(\mathbf{r}, \mathbf{u}, t)$, in which the unit vector $\mathbf{u}$ is described on a triangulated unit sphere in three-dimensional (3D) Euclidean space, and the angular Laplace operator on $q(\mathbf{r}, \mathbf{u}, t)$ is calculated using a finite volume method.[35,36] In particular, the advantage of this real-space method is that the $\mathbf{u}$-dependence is resolved in 3D and thus smectic-C phase is included in the construction of the phase diagram. However this study was limited to liquid crystalline phases with 1D spatial order, thus only smectic/lamellae phases can be touched.

Although the 1D result provides guidance for the typical microstructures of rod-coil block copolymers, some other complicated non-lamellar liquid crystalline phases discovered in experiments are beyond the capability of 1D study. Hence, efficient numerical implementations of SCFT in two (or higher)-dimensional space are greatly desirable for examining novel non-lamellar structures. Previous 2D SCFT studies by Pryamitsyn and Ganesan[29] were based on the rod-coil model with a completely rigid block for simplicity and thus chain bending conformation is ignored, however, which is the most important characteristics of semiflexible chains. In their work, the phase diagram of rod-coil block copolymers in terms of 2D space SCFT calculations on rod-coil block copolymers was constructed and several non-lamellar phases were detected. To the best of our knowledge, no SCFT study based on the wormlike chain model in high-dimensional space has been previously reported. In high dimensional space calculations, the computation intensity is enlarged greatly and enormous memory requirement is needed, which exceeds the endurance of most computing device at present. In order to cope with the computational intractability, we introduce an advanced GPGPU (general-purpose computing on graphics processing units) technology to numerically solve the chain propagator $q(\mathbf{r}, \mathbf{u}, t)$ in five-dimensional space satisfying the modified diffusion equations for semiflexible polymer chains in 2D SCFT method. In this way, the phase diagram including non-lamellar phase is constructed according to 2D space solving SCFT equations base on the wormlike chain model.

Theoretical model and numerical algorithm

We briefly outline the formulations of the SCFT for rod-coil diblock copolymers based on wormlike chain model in this section. The theoretical framework is the same as an earlier model for treating semiflexible block copolymers by Duchs and Sullivan[31] and our previous work.[35] We consider n monodisperse rod-coil diblock copolymer with an N segment number of statistical length a in a volume V. The average number density of polymers is $\rho = n/V$. Each copolymer chain is characterized by a total contour length L and a diameter D, where $L = Na$. The average volume fraction of rods and coils are f_R and f_C respectively and $f_R + f_C = 1$. The configuration of the wormlike chains are described by space curves $\mathbf{r}_i(t)$ and unit tangential vectors $\mathbf{u}_i(t) = d\mathbf{r}_i(t)/(Ldt)$, where $t \in [0, 1]$ is a chain trajectory variable and $i \in [0, n]$ identifies the i copolymer chain in multi-chain system. The rigidity of the semiflexible chain is quantified by the local curvature which is proportional to $\left(\frac{\mathbf{u}_i(t)}{dt}\right)$.

In principle the different blocks will experience orientation interactions and chemical unlike repulsive interactions, which are usually specified by Flory-Huggins interaction parameters. In the current model, we will ignore the isotropic repulsion for simplicity, *i.e.*, there is no chemical difference between rod and coil blocks. Furthermore, the polymer chain is assumed thin enough *i.e.*, $L, a \gg D$, the angle-dependent excluded-volume interaction between two segments is given by $v(\mathbf{u}, \mathbf{u}') = DL^2|\mathbf{u} \times \mathbf{u}'|$ in the Onsager model.[38] The Onsager excluded-volume interactions between any two segments including rod-rod, rod-coil and coil-coil enforce local alignment of the chains. It should be noticed that it is unnecessary to impose an additional incompressibility constraint, as is commonly done in the theory of dense copolymer melts due to the introduction of hard-core repulsion between segments in the Onsager model. Furthermore, the dimensionless bending modulus or the ratio $\xi(t) = \lambda/L$ is introduced to measure the semiflexible chains' rigidity, where λ is the persistence length over which the orientation of a polymer segment persists and L is the contour length. In the very rigid chain limit $\lambda/L \gg 1$ and in the very flexible chain limit $\lambda/L \ll 1$. The free energy functional of the system in the units of k_BT can be obtained:

$$\frac{F}{V} \propto \frac{G}{V}\left[\frac{G}{\left(\int d\mathbf{u}\right)^2}\int d\mathbf{r}\int d\mathbf{u}\int d\mathbf{u}'\phi(\mathbf{r},\mathbf{u})\phi\left(\mathbf{r},\mathbf{u}'\right)\left|\mathbf{u}\times\mathbf{u}'\right| - \frac{1}{\int d\mathbf{u}}\int d\mathbf{r}\int d\mathbf{u}W(\mathbf{r},\mathbf{u})\phi(\mathbf{r},\mathbf{u})\right] - G\ln\frac{Q}{V} + G\ln G \quad (1)$$

where $G = L^2D\rho$ indicates the orientational interaction intensity and $\phi(\mathbf{r}, \mathbf{u}) = \phi_R(\mathbf{r}, \mathbf{u}) + \phi_C(\mathbf{r}, \mathbf{u})$ is the normalized segment density field. $Q = \int d\mathbf{u}\int d\mathbf{r}q(\mathbf{r}, \mathbf{u}, 1)/\int d\mathbf{u}$ denotes the single chain partition function subjected to the mean potential field generated by other copolymers $W(\mathbf{r}, \mathbf{u})$.

The polymer segment probability distribution function $q(\mathbf{r}, \mathbf{u}, t)$ gives the probability density of finding the t-segment that starts

from the rod terminal ($t = 0$) and ends at position $\mathbf{r}$ with orientation $\mathbf{u}$. It satisfies the modified diffusion equation:

$$\frac{\partial}{\partial t}q(\mathbf{r},\mathbf{u},t) = \left[-L\mathbf{u}\cdot\nabla_{\mathbf{r}} + \frac{1}{2\xi(t)}\nabla_{\mathbf{u}}^2 - W(\mathbf{r},\mathbf{u})\right]q(\mathbf{r},\mathbf{u},t) \quad (2)$$

with the initial condition of $q(\mathbf{r}, \mathbf{u}, 0) = 1$. Similarly, the other segment probability distribution function $q^+(\mathbf{r}, \mathbf{u}, t)$ corresponds to the probability for a partial copolymer chain of length t that starts from the other end of the chain ($t = 1$) and ends at position $\mathbf{r}$ with orientation $\mathbf{u}$. It satisfies the modified diffusion equation:

$$\frac{\partial}{\partial t}q^+(\mathbf{r},\mathbf{u},t) = \left[-L\mathbf{u}\cdot\nabla_{\mathbf{r}} - \frac{1}{2\xi(t)}\nabla_{\mathbf{u}}^2 + W(\mathbf{r},\mathbf{u})\right]q^+(\mathbf{r},\mathbf{u},t) \quad (3)$$

with the initial condition of $q^+(\mathbf{r}, \mathbf{u}, 1) = 1$. According to the mean-field approximation, the following SCFT equations can be obtained by minimizing the free energy functional with respect to $\phi(\mathbf{r}, \mathbf{u})$ and $W(\mathbf{r}, \mathbf{u})$ respectively:

$$W(\mathbf{r},\mathbf{u}) = 2G\int d\mathbf{u}'\phi(\mathbf{r},\mathbf{u}')|\mathbf{u}\times\mathbf{u}'| \quad (4)$$

$$\phi_{\mathrm{R}}(\mathbf{r},\mathbf{u}) = \frac{V}{Q}\int_0^{f_{\mathrm{R}}} dtq(\mathbf{r},\mathbf{u},t)q^+(\mathbf{r},\mathbf{u},t) \quad (5)$$

$$\phi_{\mathrm{C}}(\mathbf{r},\mathbf{u}) = \frac{V}{Q}\int_{f_{\mathrm{R}}}^{1} dtq(\mathbf{r},\mathbf{u},t)q^+(\mathbf{r},\mathbf{u},t) \quad (6)$$

$$\phi(\mathbf{r},\mathbf{u}) = \phi_{\mathrm{R}}(\mathbf{r},\mathbf{u}) + \phi_{\mathrm{C}}(\mathbf{r},\mathbf{u}) \quad (7)$$

Eqn (2)–(7) constitute a set of SCFT equations describing the statistical thermodynamics of semiflexible diblock copolymers modeled by wormlike chain. The procedure of solving this set of equations is quite similar to that of Gaussian chains. Randomly generated $W(\mathbf{r}, \mathbf{u})$ will be substituted into eqn (2) and (3) and, thus, the end-segment distribution functions $q(\mathbf{r}, \mathbf{u}, t)$ and $q^+(\mathbf{r}, \mathbf{u}, t)$ can be obtained by solving modified diffusion equations. Then the block densities, $\phi_{\mathrm{R}}(\mathbf{r}, \mathbf{u})$ and $\phi_{\mathrm{C}}(\mathbf{r}, \mathbf{u})$, are calculated according to eqn (5) and (6) and potential field $W(\mathbf{r}, \mathbf{u})$ will be updated with new density using eqn (4) and (7). This process will be iterated until the difference between two successive field values can be neglected, *i.e.* the free energy and field are self-consistent.

As mentioned above, variety of analytical and numerical methods have been used to solve the modified diffusion eqn (2) and (3) for semiflexible polymer chains.[30,31,35] Most of these previous studies however are based either on further assumptions about the chain rigidity or on a spectral-method, which has been restricted to the ordered phases with axial-symmetries, such as the nematic and smectic-A phases at present. To distinguish smectic-C from smectic-A, our previous work[35] introduced the real-space numerical method, which treats the segment orientation on a unit spherical surface discretized with an icosahedron triangular mesh to circumvent the "pole problem" due to the use of the spherical coordinate system. With such an icosahedron triangular mesh, the rotational diffusion operator $\nabla_{\mathbf{u}}^2$ can be solved using real-space based finite volume algorithm also adopted in our previous papers.[35,39] Therefore, diffusion eqn (2) and (3) with two additional internal coordinates to describe the segment orientation can be solved in real space by performing a forward time centered space scheme and a finite volume algorithm for $\nabla_{\mathbf{u}}^2 q(\mathbf{r}, \mathbf{u}, t)$. We only present a brief introduction of the numerical method here and more details can be found in our previous work.[35]

In this paper, we will extend this real-space numerical method to two dimensional variation of polymer density, denoted by x–z plane with $L_x \times L_z$ lattice points with periodic boundary conditions in x- and z-directions, to do further investigations of liquid crystal behavior of rod-coil block copolymers including non-lamellar structures. We minimize the free energy F with respect to both L_x and L_z to minimize the influence of the simulation box sizes in x- and z-directions, and each minimization of the free energy is iterated with respect to a range of L_x and L_z: $(0.5\sim2)d/L$, where d is the period of the ordered phase. Furthermore, in order to obtain solutions of nematic and various smectic structures with different orientational characteristics, the calculation begins with an initial angle between the nematic director $\mathbf{n}$ and the z-axis, which ranges from 0 to $\pi/2$ by a step of $\pi/18$ but with randomly initial fields for the composition. In this work, the nematic director $\mathbf{n}$ is fixed in the z-axis direction for smectic-A structure. The final stable phase structure is thus determined as the one having the lowest free energy independent of the initial conditions. The spatial discretization is specified by $dx = dz = 0.02L$ and the contour discretization as $dt = 1/900$ to ensure that the phase structure is trustable. In this way, a 2D space phase diagram is constructed in the $f_{\mathbf{R}}$–G plane. To the best of our knowledge, it is the first time 2D space SCFT calculations for rod-coil diblock copolymers based on the wormlike chain model has been performed.

The most computationally demanding step in the SCFT algorithm described above is in obtaining $q(\mathbf{r}, \mathbf{u}, t)$ and $q^+(\mathbf{r}, \mathbf{u}, t)$ by numerically solving modified diffusion eqn (2) and (3). In contrast to the case of coil-coil diblock copolymers, the propagators $q(\mathbf{r}, \mathbf{u}, t)$ and $q^+(\mathbf{r}, \mathbf{u}, t)$ satisfy diffusion equation in the five-dimensional space composed of a two-dimensional position space $\mathbf{r}$, a two-dimensional orientation space $\mathbf{u}$ and one-dimensional time space t. Finding solutions of this five-dimensional diffusion equation presents a challenge to the polymer physics community. Firstly five-dimensional big array require allocating computing memory over 15 GBytes. To save memory, five-dimensional array is reduced to four-dimensional one by treating one of the array variable, time t, as temporary variable, which will be calculated repeatedly when it is required. Therefore, it can certainly be a challenge to computing efficiency. In this paper, GPGPU computing by taking advantage of a C-based parallel computing programming interface called CUDA (compute unified device architecture) introduced by video card manufacturer NVIDIA is adopted to numerically solve 2D SCFT equations. The GPU with great floating-point operating capability and high-memory bandwidth offers an effective and high-performance platform for coping with large computational quantity. By migrating our code to a NVIDIA GTX285 GPU, the solving procedure of the modified diffusion equations in five-dimensional space has been accelerated about 5.3 times compared to the single CPU core of Lenovo R510 server.

Results and discussion

As a first application of this 2D real-space implementation of the SCFT for semiflexible polymer system, we reexamine the self-assembly of rod-coil diblock copolymers in 1D space calculations

with the same parameters as our previous work for comparison.[35] The diblocks are specified only by the chain rigidity, that is $\xi_R = 10.0$ ($0 \le t \le f_R$) and $\xi_C = 0.1$ ($f_R < t \le 1$) for rods and coils respectively. The phase transition is induced by the pure entropic effects and the interaction strength is characterized by the parameter G. Different phases can be classified in terms of two order parameters: one is the position- and orientation-dependent densities $\phi(\mathbf{r}, \mathbf{u}) = \phi_R(\mathbf{r}, \mathbf{u}) + \phi_C(\mathbf{r}, \mathbf{u})$ and the other is the orientational order parameters characterizing the orientational structure, $\bar{P}_{1,\beta}(\mathbf{r})$ and $\bar{P}_{2,\beta}(\mathbf{r})$, where β indicates the segment species, namely rods or coils.

$$\bar{P}_{1,\beta}(\mathbf{r}) = \frac{\int d\mathbf{u}\phi_\beta(\mathbf{r},\mathbf{u})\cos\theta}{\int d\mathbf{u}\phi_\beta(\mathbf{r},\mathbf{u})}$$
$$\bar{P}_{2,\beta}(\mathbf{r}) = \frac{\int d\mathbf{u}\phi_\beta(\mathbf{r},\mathbf{u})\left[\frac{1}{2}(3\cos^2\theta - 1)\right]}{\int d\mathbf{u}\phi_\beta(\mathbf{r},\mathbf{u})} \quad (8)$$

where θ is the angle between a segment axis and the nematic direction $\mathbf{n}$ and, hence, the orientational order parameters in eqn (8) are measured from $\mathbf{n}$. The preferred orientation direction of the rod block, *i.e.*, nematic director $\mathbf{n}$ can be determined by the peak position of $\phi_\beta(\mathbf{r}, \mathbf{u})$ in eqn (5) and (6). $\bar{P}_{1,\beta}(\mathbf{r})$ describes the average spatial direction in which segments β are oriented along $\mathbf{n}$, $\bar{P}_{2,\beta}(\mathbf{r})$ characterizes the overall degree of orientational ordering along $\mathbf{n}$. Isotropic and nematic phase, with a uniform spatial distribution of density, are distinguished by $\bar{P}_{2,\beta}(\mathbf{r}) = 0$ for isotropic and $\bar{P}_{2,\beta}(\mathbf{r}) \neq 0$ for nematic structures. In smectic structures, depending on the angle between the nematic director $\mathbf{n}$ and the lamellae normal (z-axis) direction, θ_0, smectic-A and smectic-C can be identified corresponding to $\theta_0 = 0$ and $\theta_0 \neq 0$, respectively. The half-maximums of the peaks in the density distribution are employed as a boundary of the rod-rich region and coil-rich region and all of the phase region size in our following discussions is measured with full-width-half-maximum (FWHM) without special announcement.

To further illustrate the detailed structure of the smectic-C phase, the density distribution functions for the segment at t along the chain, in terms of the spatial position z, irrespective of the orientation of the segment $\mathbf{u}$, $\varphi(z, t)$ are calculated as:

$$\varphi(z,t) = \frac{V\int d\mathbf{u}q(z,\mathbf{u},t)q^+(z,\mathbf{u},t)}{Q\int d\mathbf{u}} \quad (9)$$

where several values of t include $t = 0$ (rod terminals), $t = f$ (junctions) and $t = 1$ (coil terminals).

Phase diagram from 2D calculations

According to the SCFT solutions in 2D positional space (composition variation in 2D x–z plane), the phase diagram of rod-coil diblock copolymers is constructed in the plane of orientational interactions *versus* the volume fraction of rod block (G–f_R) presented in Fig. 1a. Polymer density varying only along one dimensional (1D) space is given in Fig. 1b for comparison. In the phase diagram, typical liquid crystal phases like isotropic, nematic, smectic-A and smectic-C by taking advantage of the consideration of orientation $\mathbf{u}$ in 3D space are found at different values of G and f_R. In the Onsager model, rods tend to pack parallel or antiparallel to the nematic direction $\mathbf{n}$ to relieve the steric constraint due to the rigidity of chains therefore many phases which are common in coil-coil copolymer self-assembly such as spherical phase and bicontinuous phase are not observed for rod-coil system, but instead various liquid crystalline structures with specific chain orientation occur. From 2D phase diagram in Fig. 1a, when the rod fraction is relatively high, phase transitions including isotropic to nematic, nematic to smectic-A and smectic-A to smectic-C are all observed, which is in agreement with our previous 1D spatial calculation.[35] Furthermore, like the 1D phase diagram, the liquid crystalline interactions stabilize planar interfaces, leading to a larger lamellar region including smectic-A and smectic-C structures in the phase space due to severe steric constraints, which is different from conventional coil-coil diblock copolymers and side chain liquid crystalline block copolymers.[40] Therefore, 1D structure such as smectic phases occurs in this region of the phase diagram and can be obtained just using 1D calculation. In this case, the results by 2D calculation will be consistent with the 1D phase diagram, which is trustable in this region accordingly.

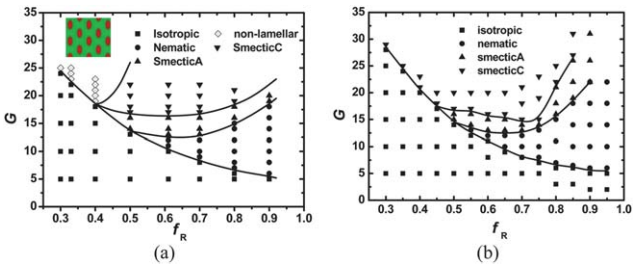

Fig. 1 Phase diagram of rod-coil diblock copolymers in the f_R–G plane from (a) 2D calculation. (b) 1D calculation in our previous paper.[35] The solid lines are a guide to the eye.

As pointed out by Pryamitsyn and Ganesan,[29] one of the advantages of 2D calculation, there is more opportunity to relieve the strain arising from the finite box size effect during the numerical procedure in search of equilibrium states, thus the smectic phases can be formed more readily. As a result, we believe that Fig. 1a provides a more accurate prediction of phase transitions for rod-coil block copolymers compared with our previous 1D phase diagram in Fig. 1b.[35] A direct comparison of the phase diagram from the 1D in our previous paper[35] and 2D numerical implementations of SCFT is demonstrated in Fig. 2. Smectic-C phase with tilt angle with respect of lamellae normal, *i.e.*, the z-axis direction $\theta_0 = 70°$, for parameter values of $f_R = 0.6$ and $G = 20$ in 2D calculation (x–z plane) is examined in Fig. 2a as a concrete example. For the same chosen parameters, the smectic-A phase was found in the SCFT simulations by Duchs and Sullivan[31] who used spherical-harmonic series to represent orientation dependent functions but limited to consider smectic-A phase for the numerical calculation to be tractable. From Fig. 2b and 2c, the density distributions as well as the orientational order parameters of rods and coils show excellent agreement between 1D and 2D calculations. Fig. 2b shows relatively strong segregation of rods and coils and coils are almost completely expelled from the middle of the rod domain. The rods

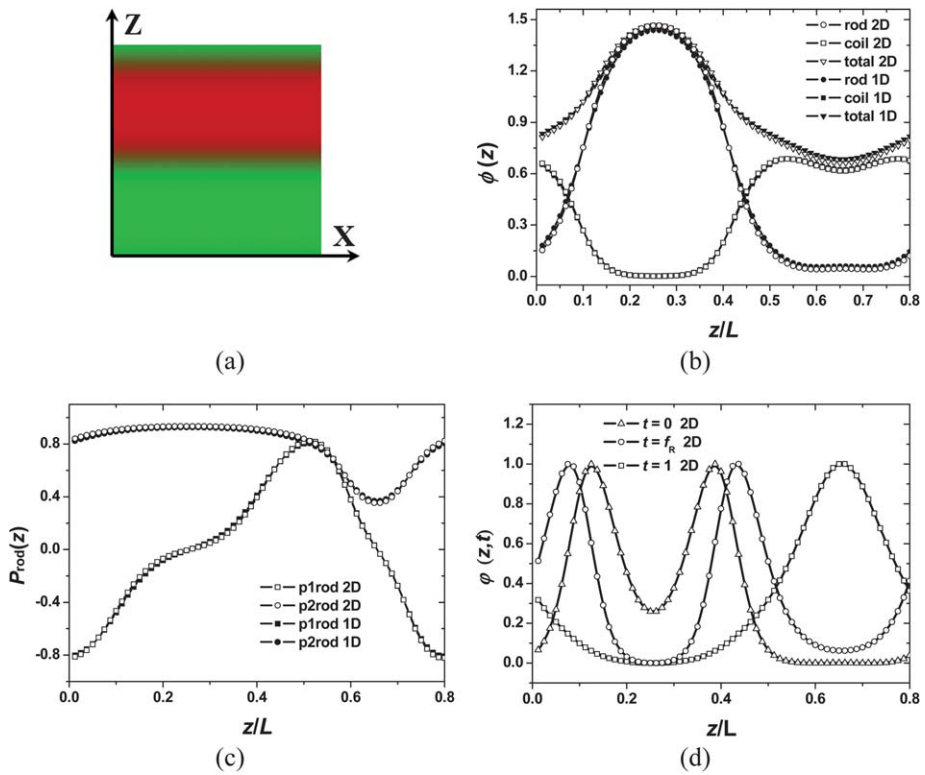

Fig. 2 Segment density and orientational order parameter distributions of a smectic-C phase with tilt angle $\theta_0 = 70°$ for $f_R = 0.6$, $G = 20$, $\xi_R(t) = 10$ and $\xi_C(t) = 0.1$ in an equilibrium calculation box of $0.8L \times 0.8L$. Figure 2b, 2c and 2d are the density and orientational order parameter distributions along the z-axis shown by the arrow in Figure 2a. In (b), (c) and (d), the text 1D and 2D in the legend indicates results from the 1D and 2D numerical calculations, respectively. (a) Red and green colors represent rods and coils, respectively. (b) Density distribution of rods $\phi_R(z)$, coils $\phi_C(z)$, and the sum of them $\phi(z) = \phi_R(z) + \phi_C(z)$. (c) Orientational distribution of $\bar{P}_{1,rod}$ and $\bar{P}_{2,rod}$. (d) Segment density profiles of $\varphi(z, t = 0)$ at rod terminals, $\varphi(z, t = f_R)$ at the rod-coil junction point, and $\varphi(z, t = 1)$ at the coil terminals.

are highly orientated and aligned with the nematic director, **n** (with a tilt angle $\theta_0 = 70°$ with respect to the z-axis direction). The thickness of rod-domain in Fig. 2a is $0.32L$, which is greatly larger than the projection length of the rod blocks in z-direction with a tilt angle 70°, $0.6L \times \cos 70° = 0.21L$. Fig. 2d shows that the segment density of the rod terminals, $\varphi(z, t = 0)$, exhibits two maxima separated by a distance of $0.26L$, which is slightly less than the thickness of the rod domain in z-direction, $0.31L$. At the same time, the segment density distribution of the junctions ($t = f$) exhibits two peaks that are separated by a distance of $0.36L$, which is slightly larger than the rod length. This observation suggests a large degree of interdigitation of the rod blocks almost exhibiting rod monolayer structure, which makes the density peaks of rod terminals and junctions occur on the interface and is consistent with the conclusions in our previous 1D calculation.[35]

A significant difference between 2D and 1D phase diagram is that a small corner at high values of G for relatively low rod volume fraction is occupied by non-lamellar phase as shown in Fig. 1a. With the increase of G, an isotropic to non-lamellar transition is obtained in the region $f_R \leq 0.4$ due to the increase of the coils' stretching entropy, instead of an isotropic to smectic-C transition predicted in our previous 1D calculation in Fig. 1b.[35] This observation is in agreement with 2D SCFT calculation for complete rigid rod-coil block copolymers by Pryamitsyn and Ganesan,[29] The isotropic-non-lamellar transition boundary shown in Fig. 1a moves up sharply with the decreasing of the rod fraction. It is reasonable that much larger values of G are needed for driving phase separation at lower f_R. Furthermore, the isotropic to non-lamellar transition is a first order transition like most order-disorder phase transitions for liquid crystalline system. According to the free energy curve of the equilibrium state for $f_R = 0.4$, as G increases, both the free energies of isotropic phase and non-lamellar phase increase linearly, as

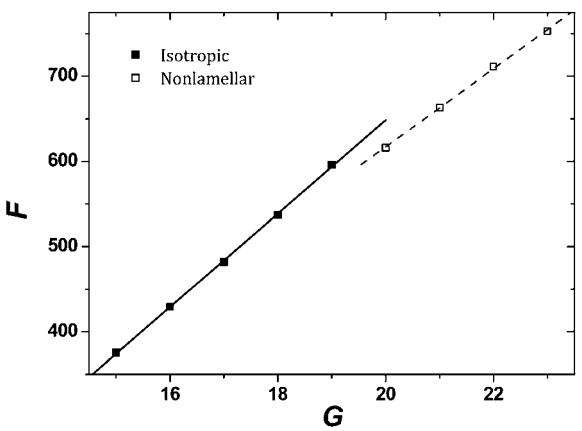

Fig. 3 Free energy F in the units of k_BT of equilibrium state according to SCFT calculations for isotropic (solid box) and non-lamellar tetragonal packing elliptic rod domains (empty box) as a function of G.

shown in Fig. 3. A significant discontinuous point emerges at the phase transition and the fitting lines of free energy for isotropic and non-lamellar phases considerably differ in slope.

Non-lamellar phase

One distinct advantage of 2D spatial calculation is that non-lamellar phases can be considered in contrast to our previous 1D work,[35,36] which can only relate to the 1D structure such as layered phases. As a concrete example, the non-lamellar structure with the rod blocks aggregated as ellipse like islands showing tetragonal packing with C4 symmetry in the coils matrix, corresponding to the "pucked phase" or "elliptical cylinders" in 3D space occurs at $f_R = 0.4$ for $G = 20$ in Fig. 4a and $G = 23$ in Fig. 4b. This structure is inherently two dimensional with a free energy lower than the smectic phases observed in the corresponding 1D phase diagram. Similar structures have been found in previous experiments done by Radzilowski *et al.*[12,13] and by Cho *et al.*[18] who also found body-centered tetragonal packing structure. The detailed structure of tetragonal packing elliptical domains can be examined in terms of the density distribution profiles of the specific segments, like rod terminals ($t = 0$), junctions of rods and coils ($t = f_R$) and orientational order parameters.

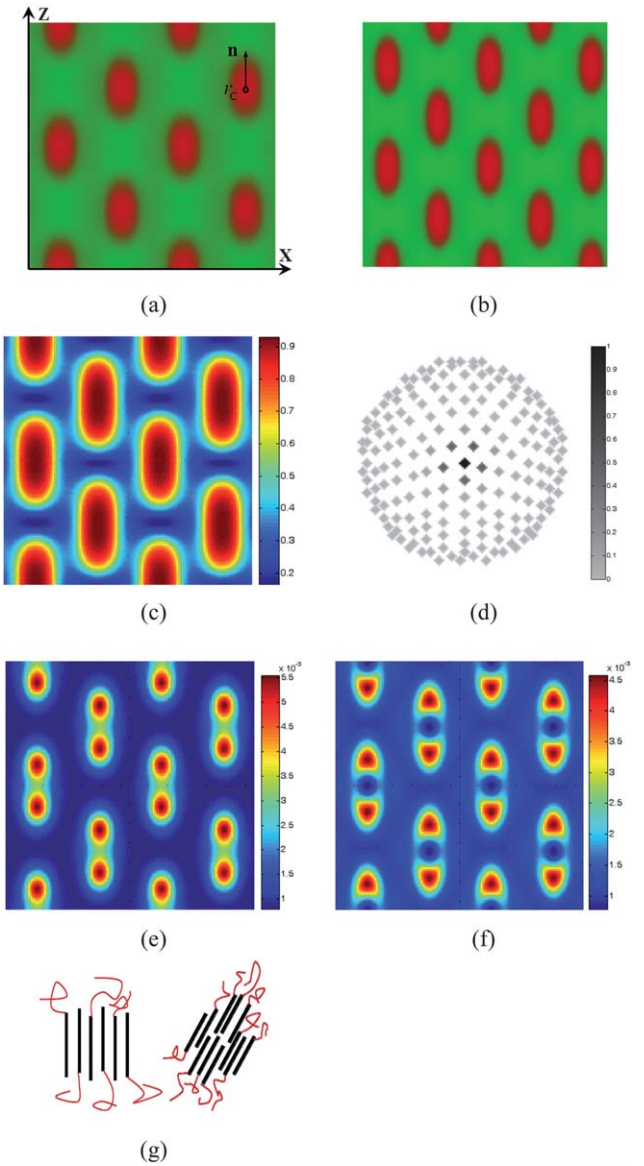

Fig. 4 Representative tetragonally packed rod cylinders in a coil matrix at rod fraction $f_R = 0.4$ for (a) $G = 20$ and (b) $G = 23$, where red and green colors represent rods and coils, respectively. Arrow on the morphology of (a) shows the nematic orientation of the rods. (c) Orientational degree of rods, $\bar{P}_{2,\mathrm{rod}}(\mathbf{r})$ corresponding to (a). (d) Orientation distribution $\phi(r_C, \mathbf{u})$ at the ellipse center r_C marked as an empty circle in (a) and $\mathbf{u}$, which is the projection of north hemisphere of icosahedron triangular grid ($z \geq 0$). The south hemisphere is reflectionally symmetric with the north one. (e) Segment density distributions corresponding to (a) for (e) the rod terminal ($t = 0$) and for (f) rod-coil junction ($t = f_R$). (g) schematic representation suggested by (e) and (f) at the left and suggested in ref. 27 on the right column.

From Fig. 4a and 4b, the ellipses' major axes are seen to be aligned parallel with each other. In this case, tetragonal packing structure has a lower energy than conventional hexagonal packing occurred in coil-coil diblock copolymers. Orientational ordering parameter $\bar{P}_{2,\mathrm{rod}}(z)$ distribution in Fig. 4c exhibits quite strong orientation degree in rod domains and elliptical shape with maxima in the core of the rod domain indicating that rods are highly orientated and aligned with the nematic director **n**. Moreover, Fig. 4d clearly shows that the orientation distribution in the center of rod domains, $\phi(r_C, \mathbf{u})$, exhibits a very sharp distribution demonstrating the nematic director **n** is along the main axis (z-axis) direction of ellipse rods. However, a hexagonally packed phase of rectangular nanodomains in the coil matrix was found at high coil volume fractions and high geometrical asymmetry between rods and coils in rod-coil (PPV-*b*-PI) system by Olsen and Segalman.[41] We should note that in their experiments, the rods are oriented randomly with quite low orientation degree. We attribute this difference to the entropy driven microphase separation and further liquid crystalline behavior in our model based on the Onsager excluded-volume interaction favoring the parallel alignment of rods. On the contrary, in the experiment work by Olsen and Segalman the microphase segregation is induced by enthalpically unlike interactions between rods and coils. In this case, Flory-Huggins unlike interaction between rods and coils dominate and the orientational interaction between rods described with Maier-Saupe interactions becomes less important, resulting in the microphase segregated morphology more like that observed in coil-coil diblock copolymers.

Fig. 4e and 4f display the density distribution of segments at $t = 0$ and $t = f_R$, corresponding to the morphology shown in Fig. 4a. The rod terminals and junctions tend to allocate only on the two ends of the ellipse's major axis and there is nearly no emergence in the middle of rod-rich domain, which implies that the rod chain arrangement adopts monolayer. Furthermore, the length of major axis of rod region in Fig. 4a is $0.47L$, which is close to the rod length of $0.4L$. This result suggests that in the elliptical rod domain of non-lamellar phase, the rods adopt almost interdigitated rod monolayer arrangements, schematically shown in Fig. 4g on the left column, rather than bilayer smectic-C or combination of bilayer and monolayer smectics as predicted by Pryamitsyn and Ganesan,[29] shown in Fig. 4g on the right column for rigid rod-coil block copolymers.

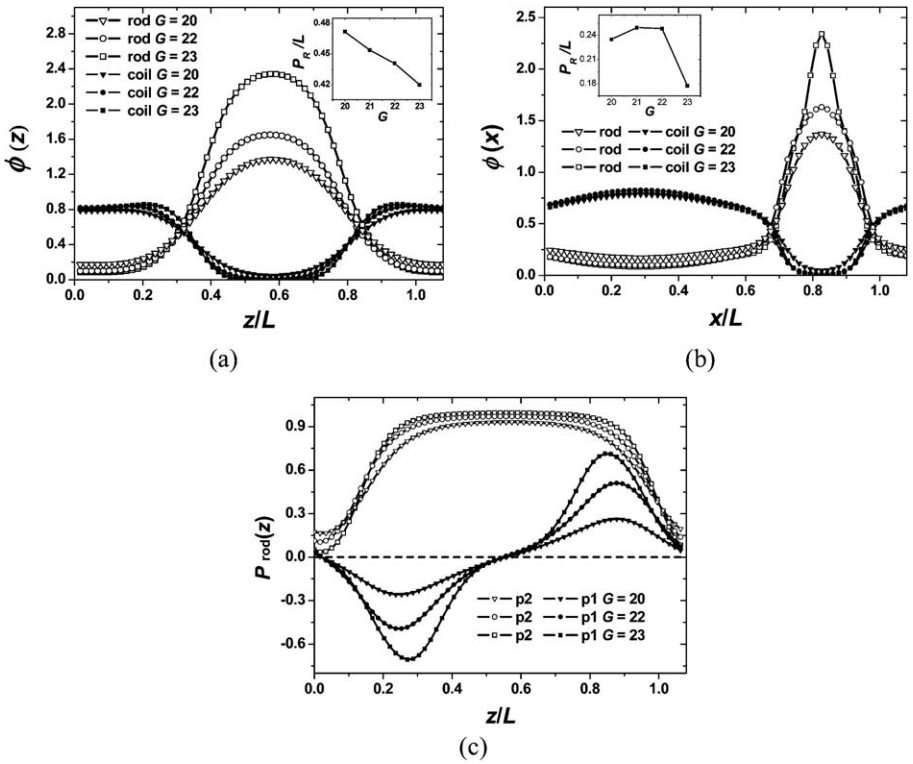

Fig. 5 Profiles for an elliptical rod domain for several values of G at $f_R = 0.4$. (a) Density profiles along elliptical major axis (z-axis) direction. (b) Density profiles along minor axis (x-axis) direction. (c) Orientational distribution of $\bar{P}_{1,\mathrm{rod}}(z)$ and $\bar{P}_{2,\mathrm{rod}}(z)$ along elliptical major axis direction. The inset in (a) and (b) denotes the variation in rod domain size, P_R, which is measured with FWHM with the increasing of G.

Fig. 5 shows the density and orientation distributions of the elliptical rod domain along the major (z-axis) and minor (x-axis) axis directions as a function of G. From Fig. 5a and 5b, one can clearly distinguish a strongly segregated rod-rich core with a sharp rod-coil interface in a coil-rich matrix. In the middle of the rod domain, the coils are almost completely expelled by densely packed rods, like the smectic-C case in Fig. 2b. With the increase of G, stronger phase-segregation for the rod and coil regions both in the major (z-axis) direction in Fig. 5a and minor (x-axis) direction in Fig. 5b is found. The coils are almost completely expelled from the middle of the rod-rich core even for relatively weak orientational interaction $G = 20$. This effect becomes more pronounced in the minor axis directions, which is manifested in the left column of Fig. 4g according to the rods arrangement. Fig. 5c shows the distribution of orientational order parameters $\bar{P}_{1,\mathrm{rod}}(z)$ and $\bar{P}_{2,\mathrm{rod}}(z)$ corresponding to Fig. 5a, which are defined in eqn (8). In the middle planes of the rod and coil domains, the average first-order orientation order orientation order parameter, $\bar{P}_{1,\mathrm{rod}}(z)$, vanishes, indicating that the rod orientation is symmetric about the nematic director **n**.

It is interesting to note that the size of the rod-rich domain in both major and minor axis directions decreases when G becomes larger, as shown in Fig. 5a and Fig. 5b. The insets in Fig. 5a and 5b show the variation in length of the major and minor axes of rod-rich cores, P_R, caused by the increasing of G. A significant decrease in P_R in both major and minor axes directions can be observed when the G values vary from $G = 20$ to $G = 23$, indicating rods packed more regular and denser in the rod-rich core with the increasing of G. This observation of phase behavior can be attributed to the competition between the excluded-volume interaction between rods and the stretching energy of the coils.[42] For coil-coil diblock copolymers, with the increase of microphase separation degree (*i.e.*, the increase of Flory-Huggins interaction parameter between different unlike species) the size of microdomains increases to reduce the interfacial energy. However, the increase of G leads to entropy driven microphase separation due to excluded volume effect. The pronounced excluded-volume effect drives the rod blocks to align more closely while the coils suffer a higher entropy penalty due to stretching, and thus resulting in the decrease of the rod size. As the orientational interaction enhances, rods tend to pack more interdigitated even forming complete monolayer smectic structures to reduce the stretching energy of coils. It is noted that by numerically solving semiflexible SCFT equations with spectral methods but without consideration of anisotropic orientational interaction between rods, Matsen[30] observed that the increase of molecular rigidity resulted in the decrease of interfacial tension and further reducing the period of layered phases and interfacial width.

Stability of zigzag structures

In the optimization of numerical implementation of SCFT for semiflexible chains as mentioned in the part of theoretical model and numerical algorithm, the free energy with respect to the size of simulation cell is found to have some local minima, corresponding to different morphologies with different orientational structures. The stable structure is chosen as the one with global

free energy minimum. According to our 2D numerical calculations, we further explore the occurrence of other layered structures, such as zigzag initially observed by Chen and coworkers[10,11] for polyhexyl-isocyanate-polystyrene (PHIC-PS) rod-coil block copolymers during solvent evaporation and defect smectic structures in rigid rod-coil diblock copolymers with SCFT simulations.[29]

Many efforts are made to determine and explain the stability of zigzag morphology in previous work.[11,28,29] Chen *et al.*[11] reported that a zigzag structure is a metastable state by using scaling analysis and the occurrence of zigzag is hypothesized as strong procedure-dependence. Comparing with uniformed smectic-C phase, lengthened rod-coil interface in zigzag morphology is obviously unfavorable to the free energy, while allowing the coils to become less stretched and hence suffering less entropy penalty. Furthermore, it only appears when good solvent is used as casting solvent, like the work by Chen *et al.*, in which conditions chemical repulsion is well screened during solvent evaporation. Li and Gersappe[28] theoretically confirmed this hypothesis by employing 2D SCFT calculation based on lattice model, in which only isotropic Flory-Huggins interactions between rods and coils are taken into consideration. Free energy analysis of the zigzag morphology, in which entropy and enthalpy are presented respectively, is in agreement with the conclusion by Chen *et al.* They predicted that the zigzag structure possibly turned to be a stable state when a Flory-Huggins interaction between rods and coils is negligible comparing with entropy effects, *i.e.*, in this case, the phase segregation is only driven by the pure entropy. Pryamitsyn and Ganesan[29] observed chevron-like defect smectic-C structures by performing 2D SCFT calculations by assuming complete rigid rods thus ignoring the bending penalty. They pointed out even the evolution was processed in a large calculation cell for a very long time, such chevron-like defects still cannot be eliminated completely. Therefore, as a concrete example, we are going to reassure the stability of zigzag morphology in pure entropy driven phase separation systems in the present article.

The zigzag morphology is given in Fig. 6a, which exhibits different periodic lengths in two directions (x–z computational cell). The result indicates that during the formation of zigzag, both the lamellae directions in two axes need to be adjusted to commensurate with the orientation of rods, which is more difficult than the evolution of smectic structures. Additionally, another similar morphology named wavy defect smectic-C is also observed under the same parameter conditions as zigzag, which is shown in Fig. 6b for comparison. Like zigzag, it is also a kind of chevron-like defect smectic structure but with a period shorter than that of zigzag. According to our numerical results for the distribution of segment density and orientation (figures not shown here), the rod blocks in zigzag and smectic-C both tilt an angle from the normal direction of lamellae and partially interdigitated in the rod-rich domain. This microstructure is qualitatively in accordance with the 1D result.[35] Differently, the zigzag has a chevron-like interface in a long distance, rather than a strictly uniform interface in defect free smectic-C shown in Fig. 6c. Clearly, the rod-coil system in the zigzag structure seems to suffer a higher interfacial energy than that of both smectic-C morphologies, while the stretching entropy of the coils is more relaxed due to a wider space for junction points of two blocks. From Fig. 6a the zigzag produces an interior angle with narrower space and an exterior angle with wider space, leading to the complicated conformation entropy of the system.

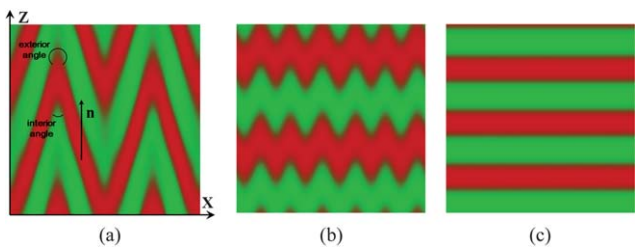

Fig. 6 Several typical morphologies in the optimization of numerical implementation of SCFT with respect to the size of 2D simulation cell with same parameters of $f_R = 0.6$ and $G = 20$. (a) Zigzag structure. (b) Defect wavy smectic-C. (c) Perfect smectic-C with the lowest free energy. Red and green colors represent rods and coils, respectively.

According to our 2D solution of SCFT equations, it is the most reliable determination of the thermodynamic stability of various structures by comparing their free energies. For instance, the dimensionless free energy per volume of perfect smectic-C phase at $G = 20$, $f_R = 0.6$ and $G = 21$, $f_R = 0.6$ are 446.48 and 474.27 respectively, while those of zigzag phase are 454.19 and 480.31. The free energy is in the units of k_BT. By comparing the free energies for different morphologies at a series of G and f_R (for concision of the article only two typical examples are presented above), it is clear that the zigzag morphology is not a stable state for rod-coil copolymers in all explored parameters G and f_R. The coexistence region of zigzag and smectic-C is only observed when G is above 19 and $f_R \geq 0.5$. When the cell size for 2D calculation is larger than the optimized period of layer phase, one fails to obtain a converged lamellar phase, a chevron-like zigzag morphology emerged instead.

Conclusions

In this work, a 2D positional space numerical implementation of the SCFT method is presented for semiflexible block copolymers, and an advanced GPGPU technique is introduced to cope with the computational intractability for the solution of five-dimensional chain propagator $q(\mathbf{r}, \mathbf{u}, t)$, satisfying the modified diffusion equations. The microphase separation and liquid crystalline behavior is driven only by the entropy based on the Onsager excluded-volume interaction between rods. In contrast to a Gaussian chain, due to the chain rigidity, the description of additional orientation degree of freedom of the segments $\mathbf{u}$ is needed, in this article, which is discretized by a uniform triangulated unit sphere in 3D Euclidean space. Based on this technique, the angular Laplacian is solved using a finite volume algorithm and a smectic-C phase with broken axis symmetry can be readily discerned, whereas at present the commonly adopted method related to spherical-harmonic expansions is limited to the smectic-A phase.

According to our 2D space numerical implementation SCFT for semiflexible chains, a phase diagram including non-lamellar structure besides isotropic, nematic, smectic phases in 1D spatial calculations, is constructed as a function of the rod volume fraction f_R and orientational interaction degree G. By comparing

with our previous phase diagram with 1D ordered phases under the same parameters condition, the perfect agreement is found in quite wide regions of the phase diagram with large volume fraction of rods, further confirming that the layered phases occupy a larger region in the phase space due to liquid crystalline interactions. In particular, a novel non-lamellar phase is observed in relatively low rod fraction region of the 2D phase diagram, in contrast to the smectic phases observed in the corresponding 1D phase diagram. In this non-lamellar phase, the rods are phase segregated as elliptical islands showing tetragonal packing with C4 symmetry in the coils matrix, corresponding to the "pucked phase" or "elliptical cylinders" in 3D space. The size of the rod-rich domain in both ellipse major and minor axis directions decreases when orientational interaction degree G becomes larger due to excluded-volume effect driving the rod blocks to align more closely. Furthermore, according to our 2D solution of SCFT equations, other layered structures such as zigzag and wavy lamellae are confirmed to be thermodynamically unstable by comparing their free energies. The free energies for different morphologies at several values of G and f_R clearly indicate that the zigzag morphology is not a stable state for rod-coil copolymers in our calculation, whereas the perfect smectic-C phase is stable. This phenomenon is in accordance to with other experimental and theoretical results.[11,28] In this article, only the Onsager-type orientational interaction is considered between rods to focus on the liquid crystalline behavior originated from the excluded-volume effect. It is convenient to straightforwardly extend to the inclusion of other anisotropic orientational interactions like the Maier-Saupe model suitable for thermotropic liquid crystallines.

Acknowledgements

We thank financial support from the NSF of China (Grant Nos. 20990231 and 20874020) and funding from the National Basic Research Program of China (Grant Nos. 2008AA032101 and 2011CB605700) is also acknowledged.

References

1 J. S. Liu, E. Sheina, T. Kowalewski and R. D. McCullough, *Angew. Chem., Int. Ed.*, 2001, **41**, 329–332.
2 X. Yang and J. Loos, *Macromolecules*, 2007, **40**, 1353–1362.
3 R. A. Segalman, B. McCulloch, S. Kirmayer and J. J. Urban, *Macromolecules*, 2009, **42**, 9205–9216.
4 Z. H. Nie and E. Kumacheva, *Nat. Mater.*, 2008, **7**, 277–290.
5 J. C. M. van Hest, *Polym. Rev.*, 2007, **47**, 63–92.
6 J. Huang, C. W. P. Foo and D. L. Kaplan, *Polym. Rev.*, 2007, **47**, 29–62.
7 A. J. Simnick, D. W. Lim, D. Chow and A. Chilkoti, *Polym. Rev.*, 2007, **47**, 121–154.
8 Y. Pae and F. W. Harris, *J. Polym. Sci., Part A: Polym. Chem.*, 2000, **38**, 4247–4257.
9 B. D. Olsen and R. A. Segalman, *Mater. Sci. Eng., R*, 2008, **62**, 37–66.
10 J. T. Chen, E. L. Thomas, C. K. Ober and G. P. Mao, *Science*, 1996, **273**, 343–346.
11 J. T. Chen, E. L. Thomas, C. K. Ober and S. S. Hwang, *Macromolecules*, 1995, **28**, 1688–1697.
12 L. H. Radzilowski, B. O. Carragher and S. I. Stupp, *Macromolecules*, 1997, **30**, 2110–2119.
13 L. H. Radzilowski and S. I. Stupp, *Macromolecules*, 1994, **27**, 7747–7753.
14 M. Lee, B. Cho, H. Kim, J. Yoon and W. Zin, *J. Am. Chem. Soc.*, 1998, **120**, 9168–9179.
15 K. K. Tenneti, X. Chen, C. Y. Li, Y. Tu, X. Wan, Q. Zhou, I. Sics and B. S. Hsiao, *J. Am. Chem. Soc.*, 2005, **127**, 15481–15490.
16 J. Ryu, N. Oh, W. Zin and M. Lee, *J. Am. Chem. Soc.*, 2004, **126**, 3551–3558.
17 C. Y. Li, K. K. Tenneti, D. Zhang, H. Zhang, X. Wan, E. Chen, Q. Zhou, A. Carlos, S. Igos and B. S. Hsiao, *Macromolecules*, 2004, **37**, 2854–2860.
18 B. K. Cho, Y. W. Chung and M. Lee, *Macromolecules*, 2005, **38**, 10261–10265.
19 N. Sary, L. Rubatat, C. Brochon, G. Hadziioannou and R. Mezzenga, *Macromol. Symp.*, 2008, **268**, 28–32.
20 N. Sary, C. Brochon, G. Hadziioannou and R. Mezzenga, *Eur. Phys. J. E*, 2007, **24**, 379–384.
21 C. Dai, W. Yen, Y. Lee, C. Ho and W. Su, *J. Am. Chem. Soc.*, 2007, **129**, 11036–11038.
22 X. L. Chen and S. A. Jenekhe, *Macromolecules*, 2000, **33**, 4610–4612.
23 J. G. Wang, G. P. Mao, C. K. Ober and E. J. Kramer, *Macromolecules*, 1997, **30**, 1906–1914.
24 M. Lee, B. K. Cho, H. Kim, J. Y. Yoon and W. C. Zin, *J. Am. Chem. Soc.*, 1998, **120**, 9168–9179.
25 M. Lee, B. K. Cho, H. Kim and W. C. Zin, *Angew. Chem., Int. Ed.*, 1998, **37**, 638–640.
26 M. Lee, B. K. Cho, Y. S. Kang and W. C. Zin, *Macromolecules*, 1999, **32**, 7688–7691.
27 M. W. Matsen and C. Barrett, *J. Chem. Phys.*, 1998, **109**, 4108–4118.
28 W. Li and D. Gersappe, *Macromolecules*, 2001, **34**, 6783–6789.
29 V. Pryamitsyn and V. Ganesan, *J. Chem. Phys.*, 2004, **120**, 5824–5838.
30 M. W. Matsen, *J. Chem. Phys.*, 1996, **104**, 7758–7764.
31 D. Duchs and D. E. Sullivan, *J. Phys.: Condens. Matter*, 2002, **14**, 12189–12202.
32 R. C. Hidalgo, D. E. Sullivan and J. Z. Y. Chen, *J. Phys.: Condens. Matter*, 2007, **19**, 376107.
33 M. Deng, Y. Jiang, H. Liang and J. Z. Y. Chen, *Macromolecules*, 2010, **43**, 3455–3464.
34 Y. Jiang and J. Z. Y. Chen, *Macromolecules*, 2010, **43**, 10668–10678.
35 W. D. Song, P. Tang, H. D. Zhang, Y. L. Yang and A. C. Shi, *Macromolecules*, 2009, **42**, 6300–6309.
36 W. D. Song, P. Tang, F. Qiu, Y. L. Yang and A. C. Shi, *Soft Matter*, 2011, **7**, 929–938.
37 R. C. Hidalgo, D. E. Sullivan and J. Z. Y. Chen, *Phys. Rev. E: Stat., Nonlinear, Soft Matter Phys.*, 2005, **71**, 041804.
38 A. N. Semenov and A. R. Khokhlov, *Sov. Phys. Usp.*, 1988, **31**, 988–1014.
39 P. Tang, F. Qiu, H. Zhang and Y. Yang, *Phys. Rev. E: Stat., Nonlinear, Soft Matter Phys.*, 2005, **72**, 016710.
40 M. Shah, V. Pryarnitsyn and V. Ganesan, *Macromolecules*, 2008, **41**, 218–229.
41 B. D. Olsen and R. A. Segalman, *Macromolecules*, 2007, **40**, 6922–6929.
42 M. W. Matsen and F. S. Bates, *J. Chem. Phys.*, 1997, **106**, 2436–2448.